Journal of Power Sources 195 (2010) 2050–2056

Contents lists available at ScienceDirect

Journal of Power Sources

journal homepage: www.elsevier.com/locate/jpowsour

Fabrication of carbon nanofiber-driven electrodes from electrospun polyacrylonitrile/polypyrrole bicomponents for high-performance rechargeable lithium-ion batteries

Liwen Ji, Yingfang Yao, Ozan Toprakci, Zhan Lin, Yinzheng Liang, Quan Shi, Andrew J. Medford, Christopher R. Millns, Xiangwu Zhang*

Fiber and Polymer Science Program, Department of Textile Engineering, Chemistry and Science, North Carolina State University, 2401 Research Drive, Raleigh, NC 27695-8301, USA

ARTICLE INFO

Article history:
Received 31 July 2009
Received in revised form 8 October 2009
Accepted 9 October 2009
Available online 20 October 2009

Keywords:
Electrospinning
Carbon nanofibers
Polyacrylonitrile
Polypyrrole
Lithium-ion batteries

ABSTRACT

Carbon nanofibers were prepared through electrospinning a blend solution of polyacrylonitrile and polypyrrole, followed by carbonization at 700 °C. Structural features of electrospun polyacrylonitrile/polypyrrole bicomponent nanofibers and their corresponding carbon nanofibers were characterized using scanning electron microscopy, differential scanning calorimeter, thermo-gravimetric analysis, wide-angle X-ray diffraction, and Raman spectroscopy. It was found that intermolecular interactions are formed between two different polymers, which influence the thermal properties of electrospun bicomponent nanofibers. In addition, with the increase of polypyrrole concentration, the resultant carbon nanofibers exhibit increasing disordered structure. These carbon nanofibers were used as anodes for rechargeable lithium-ion batteries without adding any polymer binder or conductive material and they display high reversible capacity, improved cycle performance, relatively good rate capability, and clear fibrous morphology even after 50 charge/discharge cycles. The improved electrochemical performance of these carbon nanofibers can be attributed to their unusual surface properties and unique structural features, which amplify both surface area and extensive intermingling between electrode and electrolyte phases over small length scales, thereby leading to fast kinetics and short pathways for both Li ions and electrons.

1. Introduction

Among various energy storage and conversation systems, high-performance rechargeable lithium-ion batteries (LIBs), with their high-energy density, long cycle life, and flexible design, are considered as effective solution to the increasing need for high-energy density electrochemical power sources [1–7]. Currently, LIBs are commercially available mainly as portable power sources for consumer electronic devices; however, there is an ever-increasing demand for higher capacity and higher power, especially for emerging large-scale applications including electric and hybrid vehicles, advanced wireless communication devices and storage systems for future power grids. This demand has promoted widespread research efforts toward developing high-capacity alternative electrode materials with long cycle life, improved safety, reduced environmental impact, and low cost [1–9].

Various types of carbon materials with different micro/macrostructures have been investigated in order to improve the electrochemical performance of LIBs [10,11]. In particular, the development of continuous carbon nanofibers (CNFs) through a combination of polymer electrospinning and subsequent thermal treatments has demonstrated advantages in terms of easy process, low cost, and environmentally benignity [12–14]. These fabricated CNFs present unique structures, such as extremely long fiber length, high surface area, and complex porous structure, creating large amount of active sites and reduced charge transport pathways. As a result, they are charming anode materials for high-performance rechargeable LIBs [12–14].

Polypyrrole (PPy) is one important conductive polymer and can be used as a precursor to produce carbon materials [15–17]. Improved electrochemical performance could be obtained if PPy-based carbon can be transformed to continuous nanofibers. However, it is difficult to obtain pure PPy-based CNFs via electrospinning because of the poor solubility and high conductivity of this polymer. Therefore, a polymer carrier must be used during electrospinning to produce conductive PPy precursor nanofibers [18]. Polyacrylonitrile (PAN) is easy to spin and can be used as a carrier to disperse conductive polymers to obtain electrospun multi-phase

* Corresponding author. Tel.: +1 919 515 6547; fax: +1 919 515 6532.
E-mail address: xiangwu_zhang@ncsu.edu (X. Zhang).

0378-7753/$ – see front matter © 2009 Elsevier B.V. All rights reserved.
doi:10.1016/j.jpowsour.2009.10.021

nanofibers [19]. In addition, PAN can also be directly heat-treated to form carbon [12–14,20], and hence electrospinning PAN/PPy bicomponent nanofibers will be a promising approach to produce high-performance CNF anodes for LIBs.

We, therefore, present here one relatively novel route to prepare CNFs that rely on the electrospinning of PAN/PPy bicomponent solutions. After carbonization, the resultant CNFs have high surface area and fast lithium charge/discharge kinetics, and they can be directly used as anodes for LIBs without adding any polymer binder or conducting additive. In this work, we incorporated these electrodes into laboratory-scale cells, which showed improved overall electrochemical performance when compared with graphite, which is presently being used in commercial LIBs. It is envisaged that this class of materials are promising electrode candidates for LIBs to meet the stringent demands of a society constantly seeking more advanced device lifetimes and energy densities.

2. Experimental

PAN, PPy and solvent N,N-dimethylformamide (DMF) were purchased from Aldrich. All these reagents were used without further purification. DMF solutions of PAN (8 wt%) containing different amounts of PPy (15, 30, and 50 wt%) were prepared at 60 °C with mechanical stirring for at least 72 h.

A variable high voltage power supply (Gamma ES40P-20W/DAM) was used to provide a high voltage (around 14 kV) for electrospinning with 0.5 ml h^{-1} flow rate and 15 cm needle-to-collector distance. The electrospun PAN/PPy bicomponent nanofibers were first stabilized in air environment at 280 °C for 3.5 h (heating rate was 5 °C min^{-1}) and then carbonized at 700 °C for 2 h in argon atmosphere (heating rate was 2 °C min^{-1}).

The morphology and diameter of PAN/PPy bicomponent nanofibers and their carbonized products were evaluated using scanning electron microscopy (JEOL 6400F Field Emission SEM at 5 kV). Thermal properties of PAN/PPy nanofibers were evaluated using differential scanning calorimetery (DSC) from 25 to 400 °C at a heating rate of 10 °C min^{-1} in a nitrogen atmosphere (Perkin Elmer Diamond Series DSC with Intracooler). Thermo-gravimetric analysis (TGA) was also used to determine the weight loss of PAN/PPy bicomponent nanofibers (after solvent evaporation) at 10 °C min^{-1} from 25 to 800 °C in air (TA Instruments Hi-Res TGA 2950). The structural variations of CNFs were identified by wide-angle X-ray

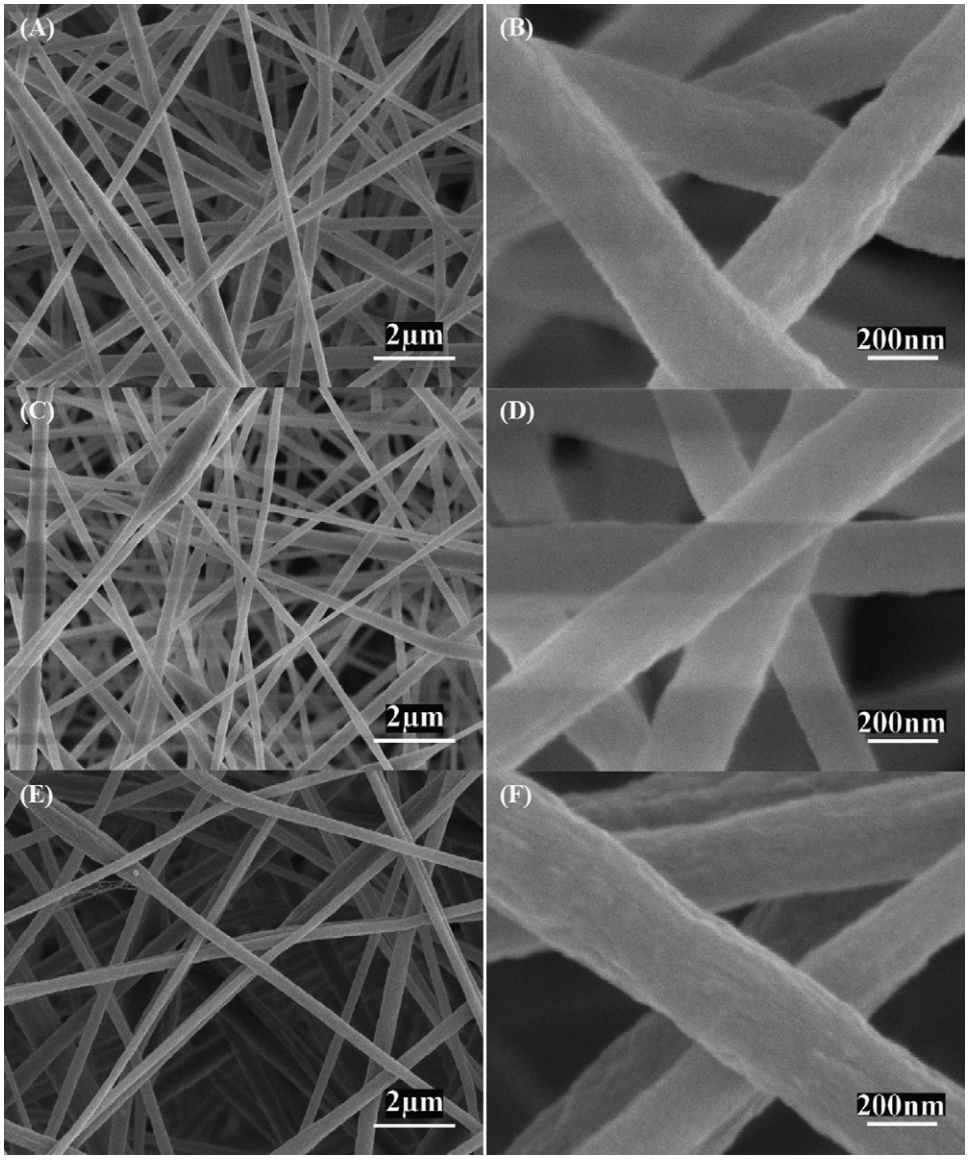

Fig. 1. SEM images of PAN/PPy bicomponent nanofibers with different PPy contents: (A and B) 15 wt%, (C and D) 30 wt%, and (E and F) 50 wt%.

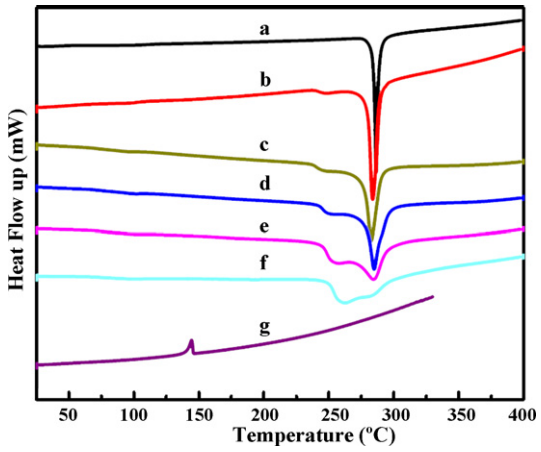

Fig. 2. DSC thermograms of PAN/PPy bicomponent nanofibers with different PPy contents: (a) 0 wt% (pure PAN), (b) 5 wt%, (c) 10 wt%, (d) 15 wt%, (e) 30 wt%, and (f) 50 wt%. For comparison, the DSC thermogram of pure PPy (100 wt%) that cannot be electrospun is also shown (g).

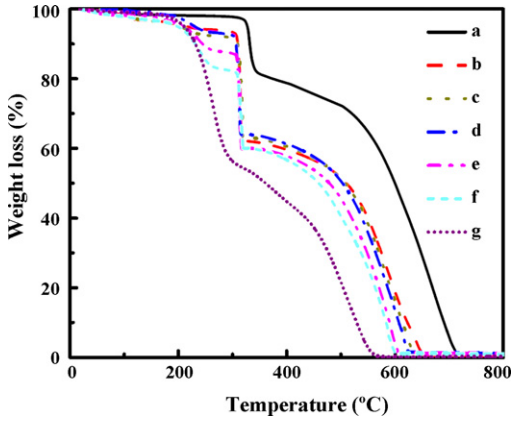

Fig. 3. TGA thermograms of PAN/PPy bicomponent nanofibers with different PPy contents: (a) 0 wt% (pure PAN), (b) 5 wt%, (c) 10 wt%, (d) 15 wt%, (e) 30 wt%, and (f) 50 wt%. For comparison, the DSC thermogram of pure PPy (100 wt%) that cannot be electrospun is also shown (g).

diffraction (WAXD, Philips X'Pert PRO MRD HR X-Ray Diffraction System, Cu kα, λ = 1.5405 Å) and Raman spectroscopy (Horiba Jobin Yvon LabRam Aramis Microscope, 633 nm HeNe Laser).

Electrochemical performance was evaluated using 2032 coin cells (Hohsen Corp.). CNFs were attached onto copper foils to be directly used as the working electrode. The loading density was around 2.5 mg per electrode. Lithium ribbon (0.38 mm thick, Aldrich) was used as the counter electrode. Separion S240 P25 (Degussa AG, 25 μm) was used as the separator. The electrolyte used was 1 M lithium hexafluorophosphate ($LiPF_6$), dissolved in 1/1 (V/V) ethylene carbonate (EC)/ethyl methyl carbonate (EMC) (Ferro Corp.). Coin cells were assembled in a high-purity argon-filled glove box. Charge (lithium insertion) and discharge (lithium extraction) were conducted using an Arbin automatic battery cycler at several different current rates between cut-off potentials of 0.01 and 2.80 V. Finally, the surface morphologies of CNF anodes after 50 charge/discharge cycles were examined with JEOL 6400F FESEM at 5 kV.

3. Results and discussion

Fig. 1 shows SEM images of electrospun PAN/PPy bicomponent nanofibers with different PPy contents (15, 30, and 50 wt%). It is seen that all nanofibers have regular and straight fibrous morphology. With the increase of PPy content, irregularities, such as so-called 'beads on a string' morphology, begin to appear [21,22]. This may be a result of the increased conductivity and viscosity of the electrospinning solutions at higher PPy contents [22,23].

Thermal properties of electrospun PAN/PPy bicomponent nanofibers are explored using DSC and TGA characterizations. Fig. 2 shows DSC results of PAN/PPy nanofibers with different PPy contents. For comparison, the DSC curve of pure PPy is also shown. PAN nanofibers show a relatively large and sharp exothermic peak at about 290 °C, which is due to the complex and multiple chemical reactions (*i.e.*, dehydrogenation, instantaneous cyclization, and crosslinking) of PAN during the process of thermal treatment via the free radical mechanism [24,25]. This exothermic peak still exists in PAN/PPy bicomponent nanofibers at 290°C, but its intensity decreases with the increase of PPy content. In addition, in PAN/PPy bicomponent nanofibers, there is also a new exothermic peak at around 250 °C. With the increase of PPy content, the intensity of this peak increases and the peak position shifts to higher temperatures. Therefore, the incorporation of PPy into PAN may influence the complex chemical reaction mechanism of PAN due to the intermolecular interaction between the protonated PPy and pendant nitrile groups of PAN [26]. The intermolecular interaction promotes the initiation of the complex chemical reactions (especially, cyclization reaction) of PAN through an ion transfer mechanism [25,27] since the initiation of the cyclization reaction through ion transfer is easier than the formation of free radicals or peroxides. As a result, an exothermic peak occurs at 250 °C. However, compared with the peak at 290 °C, the 250 °C peak is wider and the total reaction is smaller because the propagation through the ionic mechanism is slower than that via the free radical mechanism. The DSC results also reveal that pure PPy has an endothermic sharp peak at about 143 °C, which is consistent with the reported results [28,29].

TGA results are summarized in Fig. 3. It is seen that the majority weight loss of pure PAN nanofibers in air occurs in two steps starting at about 310 and 500 °C, respectively, while pure PPy exhibits major weight losses at about 210 and 410 °C, respectively. This indicates that compared with PAN component, PPy phase is easier to be degraded when thermally treated in air environment. The PAN/PPy bicomponent nanofibers begin to decompose between the decomposition temperatures of PAN and PPy. According to both DSC and TGA results, 280 °C is an appropriate stabilization temperature for PAN/PPy bicomponent nanofibers. After heat treatment in air at 280 °C, the further increase in temperature in argon makes both stabilized PAN and PPy into carbon, *i.e.*, the formation of CNFs [12–17].

Fig. 4 shows CNFs prepared from PAN/PPy precursor nanofibers with different PPy contents. It is seen that PAN/PPy-driven CNFs have undulated and wrinkled surface morphology and their diameters are slightly smaller than those of PAN/PPy nanofibers (Fig. 1), which may be due to the liberation of hetero-atoms and the densification of carbon atoms in polymer chains during the thermal treatments [23,30].

The structure of CNFs produced from PAN/PPy precursors with different PPy contents was studied using WAXD (Fig. 5) and Raman spectroscopy (Fig. 6), respectively. From WAXD patterns shown in Fig. 5, it is seen that all nanofibers show a typical carbon peak at near $2\theta = 25°$, which can be ascribed to the (0 0 2) graphite layers [12,23,24]. The Raman spectroscopy (Fig. 6) shows well-known D-band at around 1350 cm^{-1} and G-band at 1600 cm^{-1}. The peak at 1350 cm^{-1} is attributed to defects and disordered portions of carbon and the peak at 1600 cm^{-1} is indicative of ordered graphitic crystallites of carbon [12,13,20,23,24]. From Fig. 6, it is seen that the D peak is always greater than the G peak for all CNFs, indicating that these CNFs are mainly hard (non-graphitized) carbons containing significant amount of disordered sections and defects. In

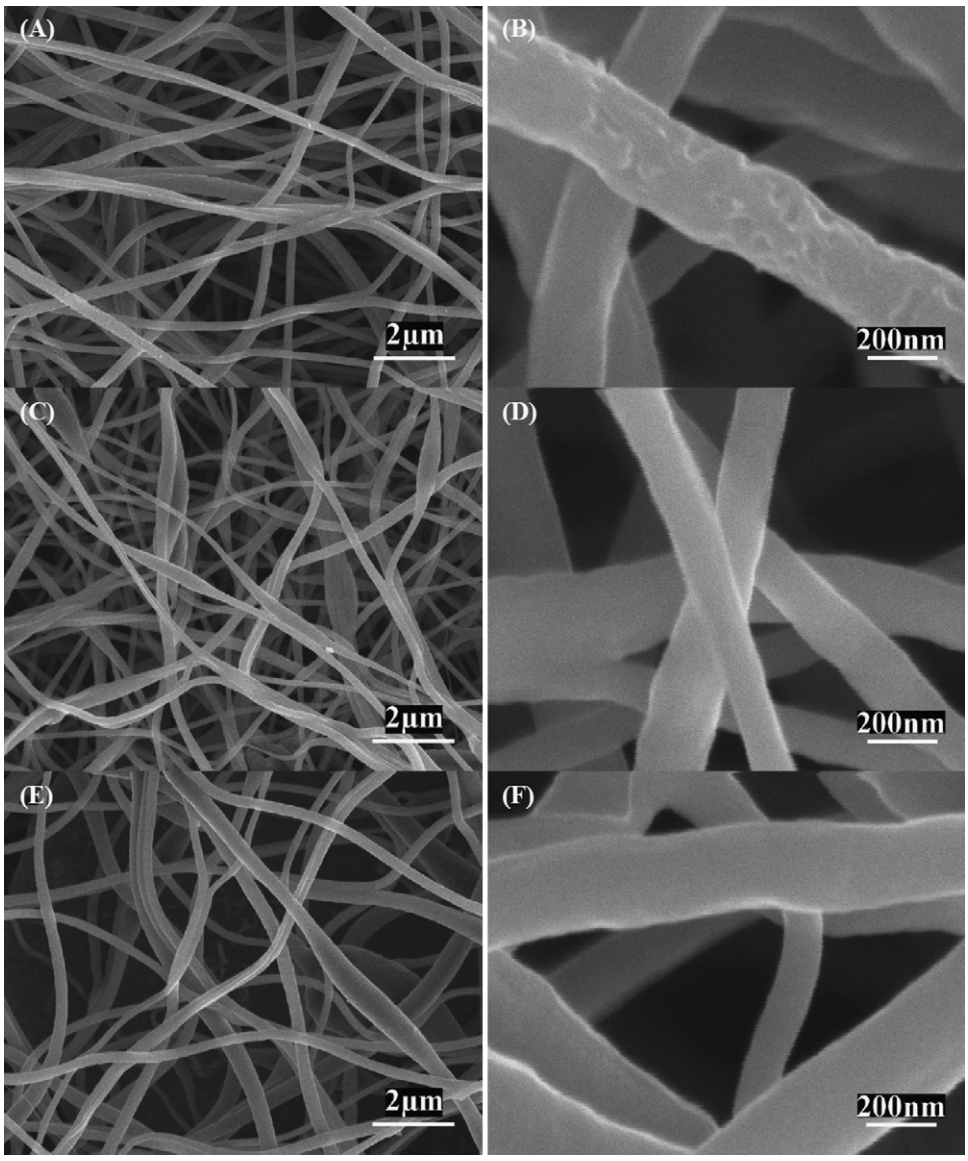

Fig. 4. SEM images of CNFs prepared from PAN/PPy precursors with different PPy contents: (A and B) 15 wt%, (C and D) 30 wt%, and (E and F) 50 wt%.

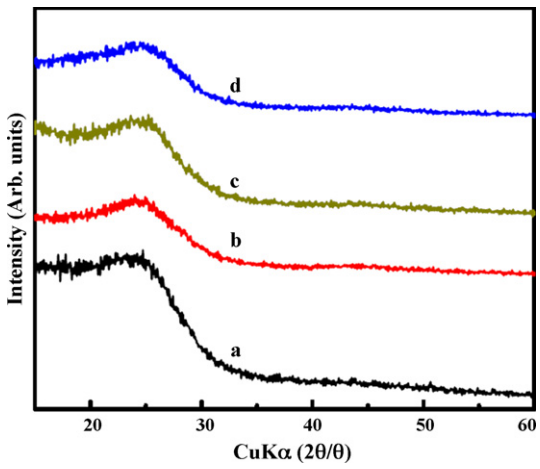

Fig. 5. WAXD patterns of CNFs prepared from PAN/PPy precursors with different PPy contents: (a) 0 wt%, (b) 15 wt%, (c) 30 wt%, and (d) 50 wt%.

addition, the integrated intensity of D peak increases slightly with the increase of PPy content, and hence the presence of PPy phase in precursor helps create more defects or disordered carbon in the resultant CNFs [12,13,20,23,24].

CNFs prepared from PAN/30 wt% PPy bicomponent precursor are used as anodes to assemble lithium-ion half cells without adding any polymer binder or conductive additive. Galvanostatic charge–discharge experiments were carried out to evaluate the electrochemical performance of these CNFs in half cells. Fig. 7 displays the charge–discharge curves and cycling performance of CNFs under a constant current rate of 0.13 C (50 mA g^{-1}) with a potential window from 0.01 to 2.8 V. As shown in Fig. 7A, during the first charge, the voltage of CNFs decreases steeply to about 0.7 V where a plateau region appear, followed by a slow decrease to the cut-off voltage. The plateau starting at 0.7 V may be assigned to the formation of a solid-electrolyte interface (SEI) layer on the electrode surface during the first charge [12,24,31]. This plateau does not appear from the second cycle, indicating that the SEI layer is relatively stable. From Fig. 7A, it is also seen that CNFs have no definite discharge plateau, which is the characteristic of the graphite anodes, because these CNFs are formed mainly by non-graphitized

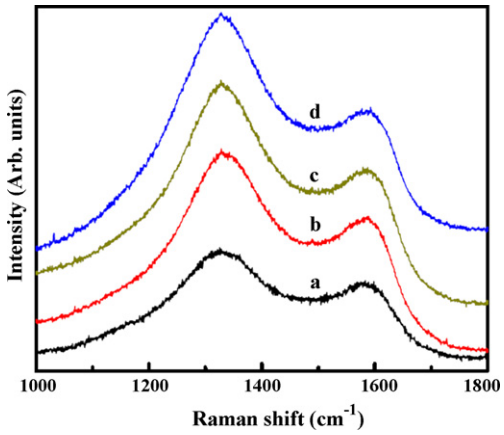

Fig. 6. Raman spectra of CNFs prepared from PAN/PPy precursors with different PPy contents: (a) 0 wt%, (b) 15 wt%, (c) 30 wt%, and (d) 50 wt%.

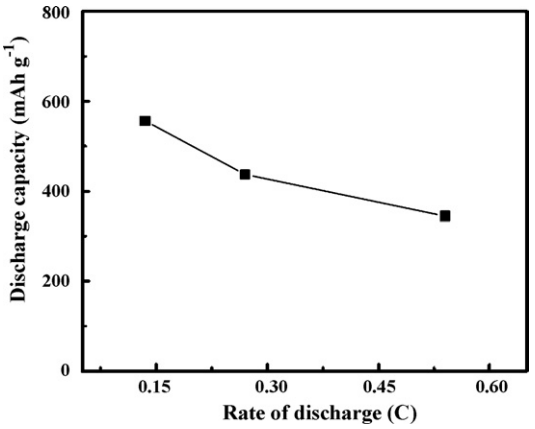

Fig. 8. Discharge capacity vs. discharge rate at the second cycle for CNFs prepared from PAN/30 wt% PPy precursor.

carbons with disordered sections and defects (see WAXD and Raman data in Figs. 5 and 6) [11–13,20–24,31–33]. In addition, the large potential difference between the charge/discharge curves may be caused by the internal resistance in the cells since the cell structure has not been optimized. From Fig. 7A, it is also seen that these CNFs deliver charge and discharge capacities of about 885 and 621 mAh g^{-1}, respectively, at the first cycle. The coulombic efficiency is about 70.2%. The discharge capacity of CNFs decreases to 556 mAh g^{-1} at the second cycle (89.5% capacity retention), and it continues to reduce to 479 and 454 mAh g^{-1} (77.1 and 73.1% capacity retention) at the 20th and 50th cycles, respectively.

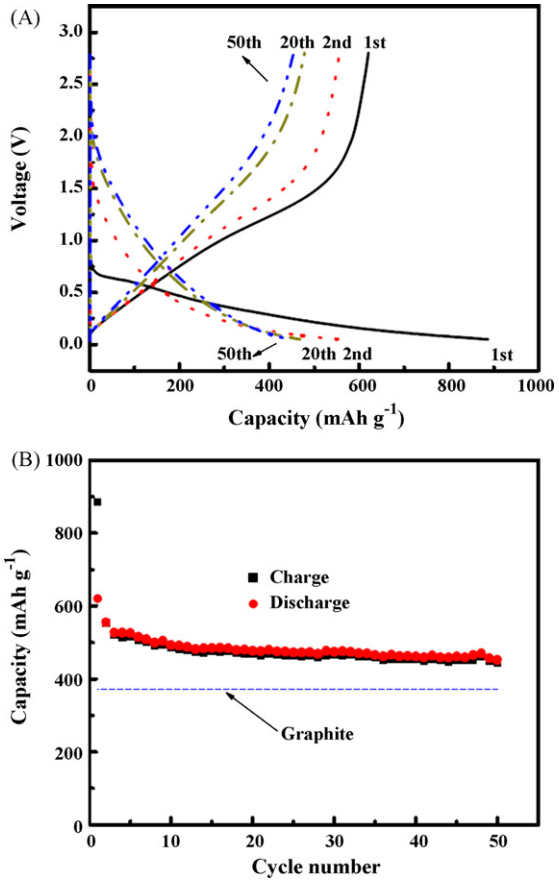

Fig. 7. Charge–discharge curves (A) and cycle performance (B) of CNFs at a constant current rate of 0.13 C (50 mA g^{-1}). CNFs were prepared from PAN/30 wt% PPy precursor. For comparison, the theoretical capacity of graphite is also shown.

Fig. 7B exhibits the cycling performance of CNFs at the current rate of 0.13 C (50 mA g^{-1}). It is seen that, at the first cycle, CNFs have an irreversible capacity of 264 mAh g^{-1} due to the formation of SEI layer. After the first charge/discharge cycle, the irreversible capacity is low and the coulombic efficiency is nearly 100%. In addition, CNFs always have much larger capacities compared with the theoretical value of 372 mAh g^{-1} of graphite [31,34–38].

Another important characteristic of these CNFs is that they can have stable electrochemical performance at relatively high current rates. The relationship between specific discharge capacity and current rate of CNFs from PAN/30 wt% PPy bicomponent precursor are shown in Fig. 8 (rate capability). It is seen that CNFs have relatively good rate capability. For example, at a current rate of 0.27 C (100 mA g^{-1}), these CNFs have a discharge capacity of about 440 mAh g^{-1} at the second cycle, which is still greater than the theoretical discharge capacity of graphite (372 mA h^{-1}). At 0.54 C current rate (200 mA g^{-1}), the capacity of these CNFs decreases slightly to 345 mAh g^{-1}. This capacity decrease can be ascribed to the formation of SEI films, limited electrode kinetics, and increased impedance at high current rates [13,20,34–37].

It is well-known that the electrochemical characteristics of carbonaceous materials strongly depend on their morphology and microstructure [4,5,12,13,20,31–37]. Compared with commercial graphite, PAN/PPy bicomponent-based CNFs have improved electrochemical performance, especially high capacities. This is probably due to their unique nanostructures and surface properties, such as disordered carbon structures, open pores, and surface defects, which can supply extra sites to storage lithium. As a result, the charge/discharge capacities of these CNFs are larger than the theoretical value of 372 mAh g^{-1} of graphite [4,5,12,13,20,31,36–41]. In addition, these fibrous structures carbonaceous materials also can alleviate the large structural changes and accommodate the strains related to the large transformation upon charge/discharge processes [4,5,12,13,20,31,36–41]. As a result, relatively good electrochemical performance, such as large reversible capacity, improved cycle ability, and good rate capability, can be obtained. From Raman spectra results, it is also seen that compared with pure PAN-driven CNFs, the PAN/PPy bicomponent-based CNFs have more disordered microstructure, which can provide extra space for the storage of lithium and its diffusion, thereby leading to higher capacities compared with former reported results [13,31,34,37,38].

In order to understand the influence of charge/discharge process on the integrity of PAN/PPy-driven CNFs, SEM images were taken after 50 charge/discharge cycles at different current rates and the results are shown in Fig. 9. It is seen that all CNFs still

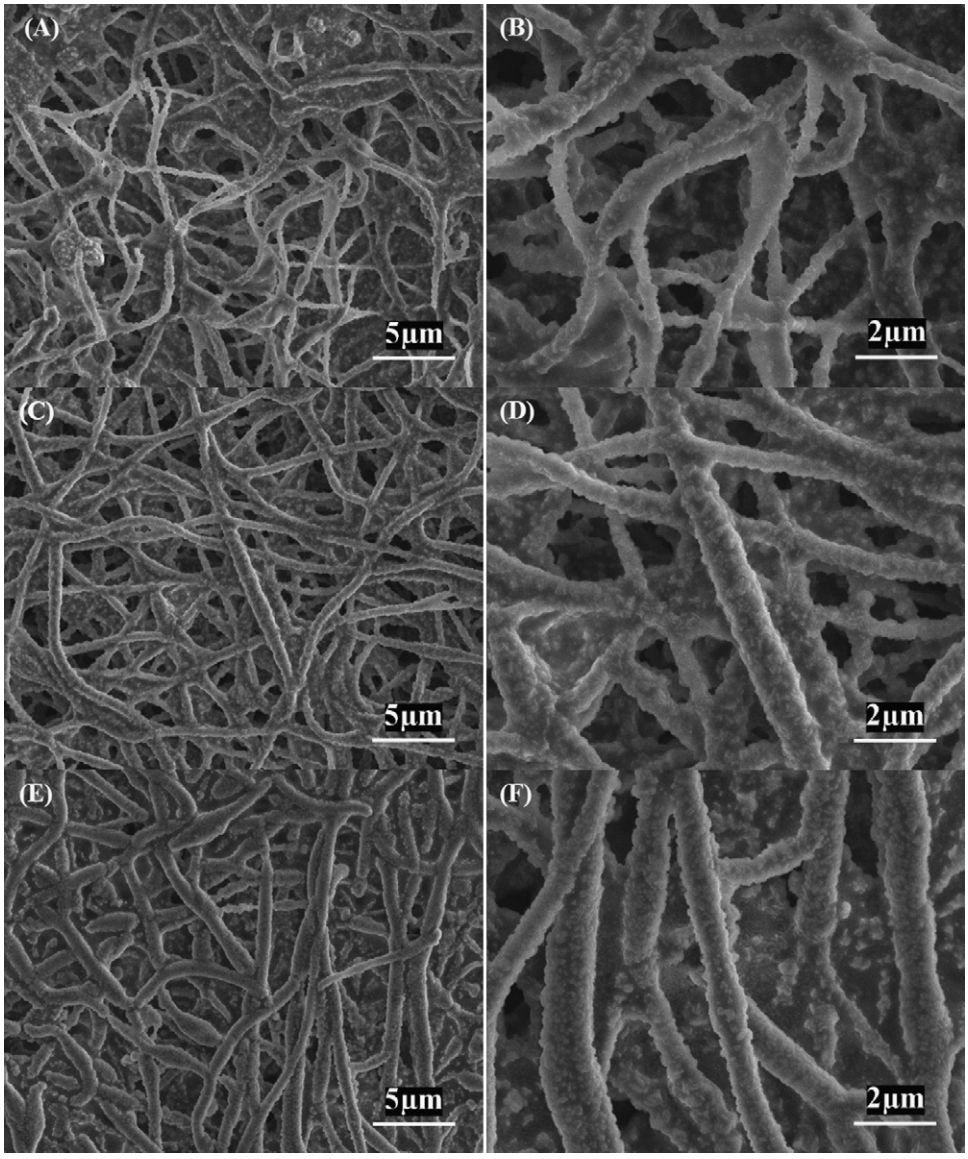

Fig. 9. SEM images of CNFs after 50 charge/discharge cycles at different current rates: (A and B) 0.13, (C and D) 0.27, and (E and F) 0.54 C. CNFs were prepared from PAN/30 wt% PPy precursor.

exhibit a relatively convoluted and wrinkled fibrous morphology after 50 cycles, indicating the integrity of CNFs is preserved during charge/discharge cycles [39,41]. These results reveal that CNFs can help LIB anodes to better withstand the volume expansion and shrinkage during lithium insertion and extraction processes.

4. Conclusion

PAN/PPy bicomponent nanofibers containing different amounts of PPy were prepared through electrospinning. SEM results show that with the increase of PPy content, the surface morphology of the fibers becomes more irregular, most likely due to the increasing solution conductivity and viscosity induced by the PPy phase. The DSC and TGA results indicate that there are some interactions between PAN and PPy phases, which influence the complex chemical reactions of PAN phase upon thermal treatment processes. After carbonization, the resultant CNFs were used as anodes for LIBs without adding polymer binder or conductive additive and they exhibit relatively large reversible capacity, good cycle performance, and high rate capability. In addition, these CNFs can maintain fibrous structure and structural integrity over 50 charge/discharge cycles. The improved electrochemical performance of PAN/PPy-driven CNFs may be caused by their large surface area for charge transfer, short distance for charge diffusion and electron conduction, and added freedom for the volume change that accompanies lithium intercalation.

Acknowledgements

This work was supported by the US National Science Foundation (Nos. 0555959 and 0833837), the ERC Program of the National Science Foundation under Award Number EEC-08212121, and ACS Petroleum Research Fund 47863-G10. The authors would like to thank Dr. Dale Balchelor, Mr. Chuck Mooney and Mr. Roberto Garcia in Analytical Instrumentation Facility at North Carolina State University and Dr. Mark D. Walters in the Shared Materials Instrumentation Facility at Duke University for their help in sample characterizations.

References

[1] J.M. Tarascon, M. Armand, Nature 414 (2001) 359–367.
[2] P. Balaya, Energy Environ. Sci. 1 (2008) 645–654.
[3] A. Manthiram, A.V. Murugan, A. Sarkar, T. Muraliganth, Energy Environ. Sci. 1 (2008) 621–638.
[4] P.G. Bruce, B. Scrosati, J.M. Tarascon, Angew. Chem. Int. Ed. 47 (2008) 2930–2946.
[5] F. Cheng, Z. Tao, J. Liang, J. Chen, Chem. Mater. 20 (2008) 667–681.
[6] Y.G. Guo, J.S. Hu, L.J. Wan, Adv. Mater. 20 (2008) 2878–2887.
[7] M.G. Kim, J. Cho, Adv. Funct. Mater. 19 (2009) 1497–1514.
[8] J. Baxter, Z. Bian, G. Chen, D. Danielson, M.S. Dresselhaus, A.G. Fedorov, T.S. Fisher, C.W. Jones, E. Maginn, U. Kortshagen, A. Manthiram, A. Nozik, D. Rolison, T. Sands, L. Shi, D. Sholl, Y. Wu, Energy Environ. Sci. 2 (2009) 559–588.
[9] A.S. Aricò, P. Bruce, B. Scrosati, J.M. Tarascon, W.V. Schalkwijk, Nat. Mater. 4 (2005) 366–377.
[10] Y.S. Hu, R.Z. Demir-Cakan, M.M. Titirici, J.O. Müller, R. Schlögl, M. Antonietti, J. Maier, Angew. Chem. Int. Ed. 47 (2008) 1645–1649.
[11] G. Zou, D. Zhang, C. Dong, H. Li, K. Xiong, L. Fei, Y.T. Qian, Carbon 44 (2006) 828–832.
[12] L.W. Ji, X.W. Zhang, Nanotechnology 20 (2009) 155705.
[13] L.W. Ji, X.W. Zhang, Electrochem. Commun. 11 (2009) 684–687.
[14] V. Thavasi, G. Singh, S. Ramakrishna, Energy Environ. Sci. 1 (2008) 205–221.
[15] S.M. Shang, X.M. Yang, X.M. Tao, Polymer 50 (2009) 2815–2818.
[16] C.M. Yang, C. Weidenthaler, B. Spliethoff, M. Mayanna, F. Schuth, Chem. Mater. 17 (2005) 355–358.
[17] X.M. Yang, T.Y. Dai, Z.X. Zhu, Y. Lu, Polymer 48 (2007) 4021–4027.
[18] I.S. Chronakis, S. Grapenson, A. Jakob, Polymer 47 (2006) 1597–1603.
[19] A. El-Aufy, Thesis, Doctor of Philosophy, Drexel University, 2004.
[20] C. Kim, K. Yang, M. Kojima, K. Yoshida, Y. Kim, Y. Kim, M. Endo, Adv. Funct. Mater. 16 (2006) 2393–2397.
[21] J.F. Zheng, A.H. He, J.X. Li, J. Xu, C.C. Han, Polymer 47 (2006) 7095–7102.
[22] L.W. Ji, A.J. Medford, X.W. Zhang, Polymer 50 (2009) 605–612.
[23] L.W. Ji, A.J. Medford, X.W. Zhang, J. Polym. Sci. Part B: Polym. Phys. 47 (2009) 493–503.
[24] C. Kim, Y. Jeong, B.T. Nhu-Ngoc, K.S. Yang, M. Kojima, Y.A. Kim, M. Endo, J.W. Lee, Small 3 (2007) 91–95.
[25] J. Kim, Y.C. Kim, W. Ahn, C.Y. Kim, Polym. Eng. Sci. 33 (1994) 1452–1457.
[26] H.S. Park, Y.J. Kim, W.H. Hong, Y.S. Choi, H.K. Lee, Macromolecules 38 (2005) 2289–2295.
[27] N. Grassie, R. McGuchan, Eur. Polym. J. 7 (1971) 1503–1514.
[28] J.M. Yeh, C.P. Chin, S. Chang, J. Appl. Polym. Sci. 88 (2003) 3264–3272.
[29] S.J. Peighambardoust, B. Pourabbas, J. Appl. Polym. Sci. 106 (2007) 697–705.
[30] H. Dong, W.E. Jones, Langmuir 22 (2006) 11384–11387.
[31] H.S. Zhou, S.M. Zhu, M. Hibino, I. Honma, M. Ichihara, Adv. Mater. 15 (2003) 2107–2111.
[32] J.R. Dahn, A.K. Sleigh, Hang Shi, J.N. Reimers, Q. Zhong, B.M. Way, Electrochim. Acta 38 (1993) 1179–1191.
[33] S.H. Yoon, C.W. Park, H. Yang, Y. Korai, I. Mochida, R.T.K. Baker, N.M. Rodriguez, Carbon 42 (2004) 21–32.
[34] J.R. Dahn, T. Zheng, Y.H. Liu, J.S. Xue, Science 270 (1995) 590–593.
[35] K. Sato, M. Noguchi, A. Demachi, N. Oki, M. Endo, Science 264 (1994) 556–558.
[36] J. Chen, F. Chen, Acc. Chem. Res. 42 (2009) 713–723.
[37] L.W. Ji, Z. Lin, A.J. Medford, X.W. Zhang, Carbon 47 (2009) 3346–3354.
[38] L.W. Ji, X.W. Zhang, Electrochem. Commun. 11 (2009) 795–798.
[39] L. Wang, Y. Yu, P.C. Chen, D.W. Zhang, C.H. Chen, J. Power sources 183 (2008) 717–723.
[40] G.L. Cui, Y.S. Hu, L.J. Zhi, D.Q. Wu, I. Lieberwirth, J. Maier, K. Müllen, Small 3 (2007) 2066–2069.
[41] C.K. Chan, H.L. Peng, G. Liu, K. McIlwrath, X.F. Zhang, R.A. Huggins, Y. Cui, Nat. Nanotechnol. 3 (2008) 31–35.